Experimental study of amplitude–frequency characteristics of high-transition-temperature radio frequency superconducting quantum interference devices

X. H. Zeng,[a] Y. Zhang,[b] B. Chesca,[c] K. Barthel,[d] Ya. S. Greenberg,[e] and A. I. Braginski
Institut für Schicht-und Ionentechnik, Forschungszentrum Jülich, D-52425 Jülich, Germany

(Received 19 October 1999; accepted for publication 19 June 2000)

We measured the amplitude–frequency characteristics of radio frequency superconducting quantum interference devices (rf SQUIDs) over a temperature range between 65 and 79 K. Using the expressions derived from the recently developed rf SQUID theory, valid also at large thermal fluctuations, we determined from these data the basic parameters of high-transition-temperature superconductor (HTS) rf SQUIDs. These parameters were: (a) the high-frequency coupling coefficient between the rf SQUID and the tank circuit resonator, k, (b) the SQUIDs hysteretic parameter, β, (c) the critical current of the Josephson junction, I_c, (d) its normal resistance, R_n, and (e) its noise parameter, Γ. We found a good agreement with the values of $\beta(I_c)$ and R_n determined directly after destructively opening the SQUID loop. In accordance with the theoretical predictions, our experimental results show that at large thermal fluctuation levels ($T \cong 77$ K), rf SQUIDs with large loop inductance operate in nonhysteretic mode up to β values exceeding 3. Furthermore, we have shown that the optimal energy sensitivity is attained in the nonhysteretic mode at a value of β distinctly higher than 1. A quantitative comparison of white noise predicted by the theory with that obtained from the experiment showed a reasonable agreement. We also discussed the contribution of the phase information to the SQUID's signal and noise at optimum operation conditions, when a mixer was used as a signal detector. © *2000 American Institute of Physics.* [S0021-8979(00)08018-X]

I. INTRODUCTION

The theoretical description of the radio frequency (rf) superconducting quantum interference device (SQUID) dates back to the seminal work by Silver and Zimmerman, to the thermal fluctuation noise treatment by Kurkijärvi, and the contribution by Jackel and Buhrman.[1–4] Concise, more up-to-date descriptions can be found in rather comprehensive reviews.[5,6] This conventional theory assumed that, for the proper operation of SQUID, the SQUID's loop inductance L_s should not exceed the fluctuation-threshold inductance $L_F = (\Phi_0/2\pi)^2/k_B T$, which is about 100 pH at 77 K, where Φ_0 is the flux quantum, k_B the Boltzmann constant, and T the absolute temperature. Also, the thermal energy should be smaller than the Josephson coupling energy of the junction, i.e., $\Gamma = 2\pi k_B T/I_c\Phi_0 < 1$, where Γ is the junction (thermal) noise parameter and I_c is the critical current of that junction. However, even in SQUIDs made of conventional low-transition-temperature superconductors (LTSs), operation at $\Gamma > 1$ was observed some time ago.[6] It is also known that rf SQUIDs fabricated from high-temperature superconductors (HTSs) can operate at 77 K with large values of the SQUID loop inductance, L_s, significantly exceeding the fluctuation-threshold inductance $L_F \cong 100$ pH.[7] Furthermore, it has been shown that such large-L_s HTS rf SQUIDs can exhibit reasonably low white flux noise levels of $S_\Phi^{1/2} \cong 10\mu\Phi_0/\mathrm{Hz}^{1/2}$, even at high values of Γ, such that $\beta\Gamma > 1$.[8,9] Here, $\beta = 2\pi I_c L_s/\Phi_0$ is the rf SQUID parameter. All these experimental observations are at variance with the expectations of conventional theory, which treat thermal fluctuations as a small perturbation, and is valid for LTS rf SQUIDs when $\beta\Gamma \ll 1$ (or $L_s \ll L_F$). Such observations can be understood, however, in the framework of Chesca's theory of rf SQUIDs operating in the presence of large thermal fluctuations.[10]

The purpose of our work has been to experimentally determine the optimum operation mode of rf SQUIDs at liquid nitrogen temperatures, and to compare the results with some of the predictions of Chesca's theory. In this article, we report on the determination of SQUID parameters from the SQUID signal amplitude versus frequency curves (AFCs) measured over a range of temperatures. For LTS rf SQUIDs, the most comprehensive measurements of this type were performed at the liquid helium temperature by Shnyrkov *et al.* and by Dmitrenko *et al.*[11,12] A quantitative comparison of experiment and theory requires the determination of all pertinent rf SQUID parameters, i.e., $\beta(I_c)$, R_n, k^2, and Q_L, where R_n is the junction normal resistance, k is the coefficient of inductive coupling between the tank circuit (resonator) and the SQUID loop, and Q_L is the loaded quality factor

[a]Present address: Pennsylvania State University, Physics Department, University Park, Pennsylvania 16802.
[b]Electronic mail: y.zhang@fz-juelich.de
[c]Present address: Physikalisches Institut, Experimentalphysik II, Universität Tübingen, 72076 Tübingen, Germany.
[d]Present address: SAP AG, D-69190 Walldorf, Germany.
[e]Permanent address: Novosibirsk State Technical University, 630092 Novosibirsk, Russia.

of the tank circuit. For rf SQUIDs, the direct determination of I_c and R_n is not straightforward. It requires opening of the SQUID loop, i.e., the destruction of the device. Assuming the validity of the theory, these parameters can be calculated from AFC data and compared with those measured destructively. In this way, a comparison of theory and experiment can be performed over a range of temperatures. Furthermore, by measuring the white flux noise versus temperature, one can determine the values of SQUID parameters resulting in optimum rf SQUID performance, i.e., in the minimum of flux noise and energy resolution.

II. EXPERIMENT

A. Characterized SQUIDs

We characterized rf SQUID washers in flip-chip configuration with the flux concentrator and the superconducting coplanar resonator surrounding the concentrator, such as those described in Refs. 8 and 9. The washer and the focuser/resonator were aligned and tightly clamped together.

The coplanar resonators had an outer diameter of 13.4 mm, their resonance frequency was about 660 MHz at 77 K, and the unloaded quality factor (without SQUID) was in the range of $Q=6000-8000$. The washer rf SQUIDs had either slit loops of $10\,\mu\text{m}\times 500\,\mu\text{m}$, or square loops of $150\,\mu\text{m}\times 150\,\mu\text{m}$, and $100\,\mu\text{m}\times 100\,\mu\text{m}$. The outer diameter of the washer was 3.5 mm. Using the formula given by Fuke *et al.*, we estimated the value of the slit loop inductance to be $L_s\cong 260\,\text{pH}$.[13] The geometric inductances of the square loops were $L_s\cong 225\,\text{pH}$ and $L_s\cong 150\,\text{pH}$. The resonators with flux concentrators and the SQUID washers were fabricated from $YBa_2Cu_3O_{7-\delta}$(YBCO) thin epitaxial *c*-axis films deposited by pulsed laser deposition on separate $LaAlO_3$ substrates. The film critical temperature was $T_c\cong 90\,\text{K}$. Step–edge junctions were used in SQUID washers. Two alternate methods have been used to prepare the necessary sharp steps in the substrate. One was to use the AZ5214 photoresist and amorphous YBCO thin film as mask, and another was to use carbon thin film masks.[14,15] For the direct four-point measurement of I_c and R_n, the loops of the already fully characterized SQUIDs were opened by a sharp diamond cutter under a low-magnification microscope. The contact pads were prepared by gold evaporation at room temperature and lift off. Initially, attempts were made to open the loops using standard photolithography. However, the processing and cleaning involved a very high risk of altering the properties of step–edge junctions.

B. Measuring methods

In Fig. 1, we show the experimental setup for the transmission measurement of AFCs and of the quality factor of the resonator. Two single-turn copper coil antennae, 13 mm in diameter, served as the driving and receiver antennas, which were connected by 50 Ω cables to the HP8752A network analyzer. An attenuator and a preamplifier were inserted between the cables and the output and input ports of the network analyzer, since the rf SQUID requires a very low rf current bias and the network analyzer needs a sufficiently high input signal amplitude. The flip-chip SQUID assembly

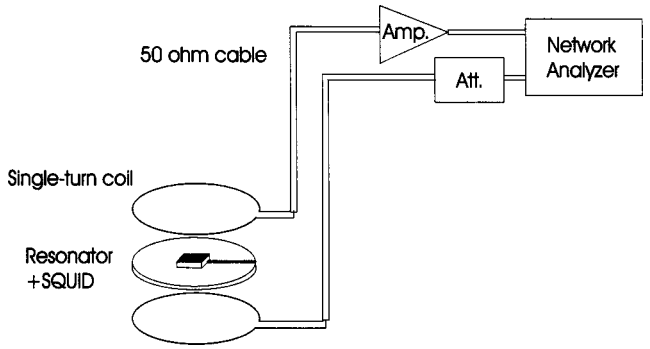

FIG. 1. Experimental setup for the transmission measurement of amplitude–frequency characteristics.

to be characterized was placed between the two coils. For the exact measurement of resonance frequency, a high quality factor of the resonator is necessary. To make the influence of the antenna coils on the resonant frequency of the resonator and quality factor negligible, the coils were very weakly coupled to the resonator. Therefore, the amplitude–frequency curves could not be measured with the optimum 50 Ω matching to the rf amplifier.

For the accurate calculation of rf SQUID parameters, the two resonance frequencies, ω_1 and ω_2, should be determined with rf power bias approaching zero. These frequencies were measured, respectively, at the external magnetic flux value of $\Phi_e=n\Phi_0$, and $\Phi_e=(n+1/2)\Phi_0$, where n is an integer. With the weak inductive coupling, the effective rf power used in AFC measurements was much less than that corresponding to −95 dB set on the attenuator at an input power of the order of, but not exactly, 1 mW, and much less than the rf power necessary to produce one Φ_0 in the SQUID loop.

To measure the white flux noise versus temperature, we also operated some of our flip-chip SQUIDs in a flux-locked loop mode using appropriate, optimized rf SQUID electronics with a synchronous, phase-sensitive detector.[16,17] In this case, the measurements have been done in the reflection mode (using a directional coupler), and the optimum 50 Ω matching was attempted by adjusting the distance between resonator and the matching copper coil to obtain the highest output signal and transfer function. In comparative measurements performed to estimate the contribution of the SQUID signal phase, we also used electronics with a diode amplitude detector, which was not optimized. Noise spectra were always collected in flux-locked mode using the HP3562A dynamic signal analyzer.

All SQUID measurements were carried out in a dewar inside a three-layer mumetal® shield. A 10-turn copper coil, 20 cm in diameter, surrounded the dewar and was used to apply weak external magnetic flux levels to the SQUID. The temperature of the liquid nitrogen bath was controlled by pumping between ~65 and 79 K. Temperature stability within 0.1 K was obtained. Temperatures were measured using a resistive Pt100 probe. The starting temperature (at atmospheric pressure) was higher than 77 K, the plausible reason was the impurity of liquid nitrogen.

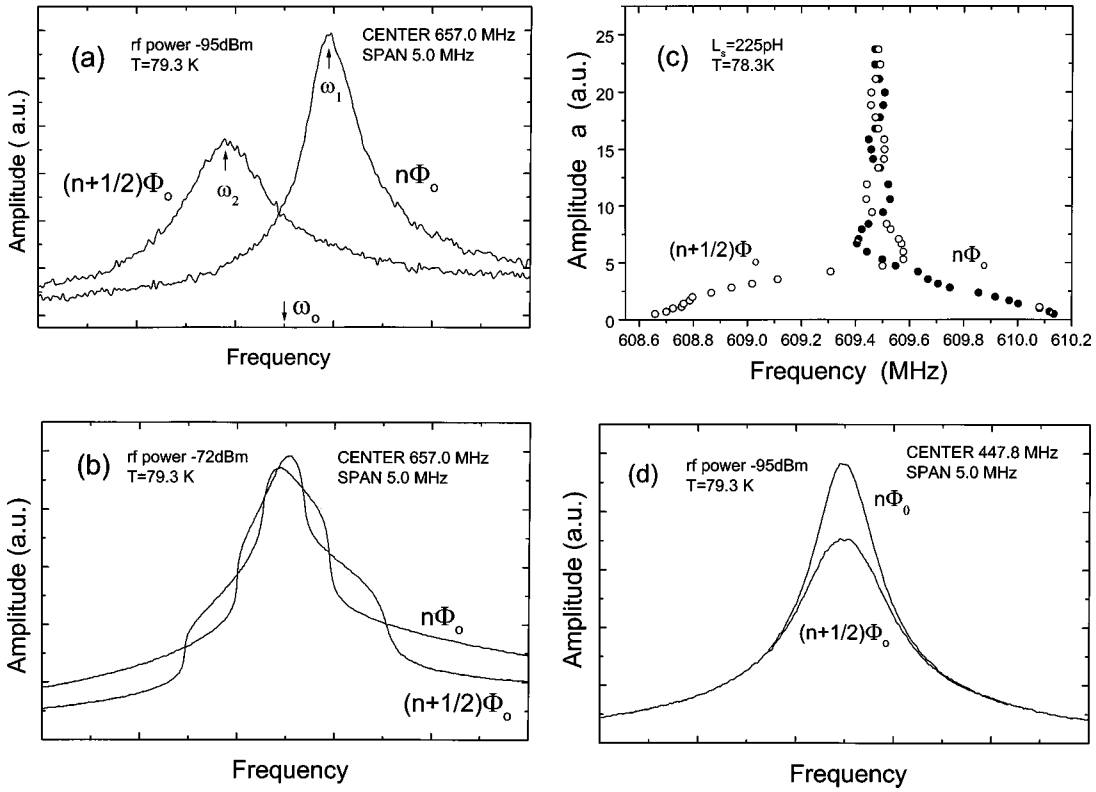

FIG. 2. (a) Two AFCs at $\Phi_e = n\Phi_0$ and $\Phi_e = (n+1/2)\Phi_0$ measured at 79.3 K, set rf power < -95 dBm, (b) Two AFCs at $\Phi_e = n\Phi_0$ and $\Phi_e = (n+1/2)\Phi_0$ measured at 79.3 K, set rf power < -72 dBm, the same SQUID as in (a), (c) rf pumping-amplitude dependence of a SQUID's resonance frequency at 78.3 K. ($L_s = 225$ pH), and (d) The AFCs of a different rf SQUID operating in hysteretic mode at 79.3 K.

The four-point measurements of junctions in opened loop included the measurement of current–voltage ($I-V$) curves and the measurement of differential resistance, dV/dI. The junction resistance can be easily determined with sufficient accuracy at high bias voltages, either from the slope of the $I-V$ curve or from the differential resistance. However, at temperatures of liquid nitrogen, due to the small critical I_c, thermal fluctuations are high ($\Gamma > 1$), and the $I-V$ curves are smooth, so that the direct determination of I_c (which is observed at a finite voltage) is not reliable. Assuming the validity of the resistively shunted junction (RSJ) model, and taking into account the high thermal fluctuations ($\Gamma \gg 1$), a good approximation of the $I-V$ curve is given by $\nu = i - i/2(i^2+\Gamma^2)$, where $\nu = V/I_c R_n$ and $i = I/I_c$ are the normalized voltage and current.[18] The normalized differential resistance $r_d = R_d/R_n$ can be expressed as

$$r_d(i) = 1 - \left[\frac{1}{2(i^2+\Gamma^2)} - \frac{i^2}{(i^2+\Gamma^2)^2} \right].$$

Since at $i=0$, $r_d(0) = 1 - 1/2\Gamma^2$. Hence, by measuring r_d at zero bias, we could determine Γ without other free parameters. From Γ we then obtained I_c. Since the expression for r_d is exactly valid when $\Gamma \gg 1$, we checked its validity when $\Gamma \geqslant 1$ by comparing our calculated $r_d(i)$ with that calculated from the full expression describing the $I-V$ curve.[18] The agreement was entirely satisfactory, within a few percent. Because of the additional noise from the electronics used to measure the $I-V$ characteristics, the differential resistance has been giving I_c values with a better accuracy than the direct fitting of $I-V$ curves. Hence, in this work, we determined $\Gamma(I_c)$ only from the measured $r_d(i)$. For accurate measurements of r_d, the excitation current must be much smaller than I_c. In our measurements, we used either 0.1 or 0.2 μA, without noticing any effect on the determined value of Γ. The measurements of R_n and r_d were performed over a range of temperatures, as in the case of SQUIDs.

III. EXPERIMENTAL RESULTS AND DISCUSSION

A. Measurements of AFCs

Figure 2(a) shows the example of two AFCs of a SQUID with $L_s \cong 260$ pH measured at $\Phi_e = n\Phi_0$ and $\Phi_e = (n+1/2)\Phi_0$. These data were obtained at the highest temperature of measurement, which was 79.3 K. The corresponding angular resonant frequencies are ω_1 and ω_2, respectively, while the resonance frequency of the resonator alone is ω_0. One can see that both the signal amplitude and the resonance frequency are modulated by the external magnetic field. Also, the quality factor at $\Phi_e = (n+1/2)\Phi_0$ is lower than that at $\Phi_e = n\Phi_0$. These data were obtained at a very low driving rf power level obtained by setting the attenuator at -95 dB at input power of the order of 1 mW. The curves represent typical characteristics of a rf SQUID in nonhysteretic (dispersive) mode, in which the rf SQUID can be seen as a nonlinear inductance, with the resonance frequency and the damping rate depending on the external magnetic flux and the external rf power level. We emphasize, again, that since the resonator and the two coil antennae were very weakly

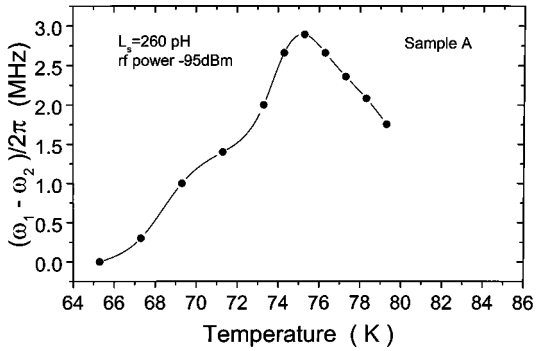

FIG. 3. Dependence of the resonant frequency difference (modulation) at <-95 dBm upon temperature. The line was drawn to guide the eye.

coupled, the real rf power applied to the resonator was much smaller than the approximate -95 dBm, which represented only a set reference value.

By increasing the driving rf power level, the difference between ω_1 and ω_2 decreases and steps begin to appear on the AFCs. With the rf power increasing further, the sign of the difference is periodically reversed. Figure 2(b) shows the analogous two AFCs of the same SQUID, which were measured at the (much higher) rf driving power level, with the attenuator set at -72 dB at the same input power as before. The AFCs show a multi valued behavior, with jumps observed as steps.

As another example, Fig. 2(c) shows the plots of ω_1 and ω_2 (on the abscissa) versus the rf voltage amplitude (corresponding to the square root of rf driving power) for a SQUID having $L_s=225$ pH and measured at 78.3 K. The solid and open circles correspond to an external flux $n\Phi_0$ (i.e., ω_1) and $(n+1/2)\Phi_0$ (i.e., ω_2). We can see that the two resonance frequencies oscillate about the resonator frequency ω_0. The oscillation amplitudes decrease with increasing rf power so that ω_1 and ω_2 gradually converge at ω_0. This result shows that the SQUID was operating in nonhysteretic mode with only one junction in the SQUID loop determining its behavior.[19]

For comparison, in Fig. 2(d) we show the AFCs of a different rf SQUID of inductance $L_s=260$ pH, which operated in hysteretic mode at the same temperature. We can see that only the signal amplitude was modulated by the external magnetic field, while the resonance frequency did not change.

In LTS rf SQUIDs with $\beta<1$ similar AFCs were predicted theoretically by Danilov and Likharev,[20] and observed experimentally by Shnyrkov *et al.* and by Dmitrenko *et al.*[11,12] The AFCs showed multivalued behavior when the product $k^2Q_L\beta>1.0$.

To measure the AFCs while increasing β (i.e., increasing the I_c of the junction) the temperature was lowered stepwise. In Fig. 3, we show an example of the temperature dependence of $(\omega_1-\omega_2)/2\pi$ at the constant low level of rf power set at about -95 dBm for a SQUID of $L_s=260$ pH. For 79.3 K and less, the resonant frequency difference increases with decreasing temperature until a maximum is reached at about 75.3 K. When lowering the temperature further, the difference decreases and becomes zero at about 65.3 K, where the SQUID enters the hysteretic regime. We note that in the nonhysteretic mode the loaded quality factor of the tank circuit measured at $\Phi_e=(n+\frac{1}{2})\Phi_0$ decreases monotonically with lowering the temperature. This is due to the effective damping increase with increasing β.

TABLE I. Parameters of a rf SQUID having $L_s\cong 260$ pH (Fig. 3) calculated from the AFCs data. Values in parentheses were measured after opening the SQUID loop.

T (K)	75.3	76.3	77.3	78.3	79.3
$k^2(\times 10^{-3})$	$\cdots$	8.0	8.14	7.46	7.92
β	(2.2 ± 0.4)	1.86	$1.63\,(1.8\pm 0.3)$	1.44	$1.24\,(1.4\pm 0.2)$
$I_c\,(\mu\mathrm{A})$	(2.8 ± 0.5)	2.4	$2.1\,(2.3\pm 0.4)$	1.8	$1.6\,(1.7\pm 0.3)$
$R_n\,(\Omega)$	(10.5)	10.7	11.86 (10.8)	11.7	12.1 (10.9)
Γ	(1.2 ± 0.2)	1.4	$1.6\,(1.4\pm 0.3)$	1.8	$2.1\,(1.9\pm 0.3)$

B. Extraction of SQUID parameters from AFC data and from the direct measurement of the junction

By extending the approach of Chesca,[10] Greenberg obtained explicit expressions for the effective damping and the effective detuning when $\Gamma>1, L_s/L_F>1$, and the driving rf power level is very low.[21] After proper simplification one obtains the following expressions:

$$\Gamma=x\frac{(1-x^2)}{\Omega}\left[1+\frac{\Omega^2}{4(1-x^2)^2}\right], \tag{1}$$

$$k^2=\frac{\omega_1-\omega_2}{\omega_0\beta x}, \tag{2}$$

$$q=\frac{Q_2^{-1}-Q_1^{-1}}{2k^2\beta x[1+(g(l)-x(1-x^2))/\Gamma]}, \tag{3}$$

where $x=\exp(-L_s/2L_F)$, $\Omega=(2\omega_0-\omega_1-\omega_2)/(\omega_1-\omega_2)$, $l=L_s/L_F$, Q_1, and Q_2 are the loaded quality factors at $n\Phi_0$ and $(n+1/2)\Phi_0$ respectively, $q=\omega_0L_s/R_n$, and $g(l)=l[1-\frac{1}{2}l+\frac{13}{72}l^2-\frac{7}{144}l^3+\frac{31}{3600}l^4-\frac{1}{1200}l^5+\frac{1}{35\,280}l^6]$. From experimental values of ω_0, ω_1, ω_2, and Q_1, Q_2, one can thus obtain Γ, β, k, and R_n.

In Table I we show the rf SQUID parameters calculated from the data of Fig. 3 and from the corresponding values of Q_1 and Q_2 measured at several temperatures. The β parameter value was 1.24 at 79.3 K and increased to 1.86 at 76.3 K, the lowest temperature of calculation. The high frequency coupling coefficient was about 8×10^{-3}, and the normal resistance was slightly less than 12 Ω. The values of $\beta(I_c)$ and R_n, given in brackets, are those determined directly from measurements after opening the loop. One can see that the agreement with values calculated from AFC data is rather good. Similar agreement was obtained for the three other SQUIDs where we opened the loop and measured junction $I-V$ characteristics conforming well to the RSJ model (the total number of tested SQUIDS was about 40, but most of the junction $I-V$ curves showed deviations from the model). This is shown in Table II, where we compare only the computed and directly measured I_c and R_n (values in brackets). The data of Tables I and II show that the use of Eqs. (1)–(3) for the determination of SQUID parameters is justified and

TABLE II. Comparison of calculated critical current and resistance of the SQUID junction with values in parentheses which were directly measured for three SQUIDs.

Device No., L_s (pH)	T (K)	I_c (μA)	R_n (Ω)
1, 150	79.3	1.7 (1.8±0.4)	7.6(8.2)
	78.3	2.2 (2.4±0.5)	7.3(8.2)
	77.3	2.4 (2.7±0.5)	6.9(8.0)
2, 260	79.3	1.7 (1.9±0.4)	11.1(12.2)
	78.3	2.1 (2.3±0.5)	9.7(12.0)
	77.3	2.6 (2.9±0.6)	9.6(11.9)
3, 260	79.3	2.0 (1.9±0.4)	14.4(11.5)
	78.3	2.3 (2.1±0.4)	11.9(11.2)
	77.3	2.5 (2.3±0.4)	9.6(11.0)

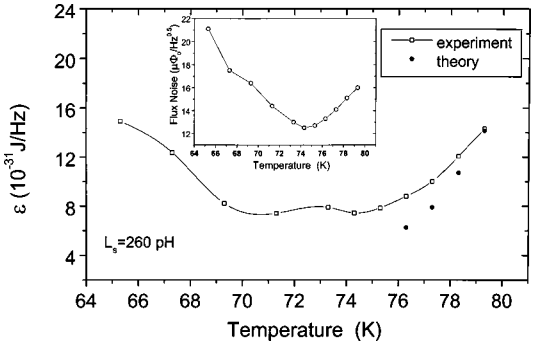

FIG. 4. Temperature dependence of energy sensitivity of the same SQUID as in Fig. 3. The line was drawn to guide the eye. The inset shows $S_\Phi^{1/2}(T)$.

that the high-thermal-fluctuation theory describes the physical reality rather well. Since the explicit expressions are valid at $\Gamma>1$ and $L_s/L_F>1$, the error could increase at $\Gamma<1$, i.e., below about 76 K. Hence, in Table I we included calculated data only for $T\geqslant 76.3$ K. By making a linear extrapolation, we estimated that our SQUID remained dispersive up to β about 3.6. This is in contrast to the low-temperature operation, in which case the transition from dispersive to hysteretic regime occurs when $\beta\cong 1$. The dispersive operation of HTS rf SQUIDs at β values, higher than 1 and up to about 3 can be inferred from Chesca's theory.

Temperature dependencies such as are shown in Fig. 3 and data of Table I are very useful in practice, as they provide the information on the optimum I_c (i.e., optimum β), and optimum temperature of SQUID operation. It will be shown in Sec. III C that the optimum performance, i.e., the minimum of flux noise, is obtained in the range where the resonance frequency modulation is maximal. For optimum operation at a different temperature, that information provides a guidance for trimming I_c, e.g., by annealing to increase or reduce the oxygen concentration in the junction.

C. Measurement of energy sensitivity

For the measurement of flux noise (S_ϕ) or energy sensitivity (ϵ), the coupling between the resonator and the receiving antenna was adjusted to improve impedance matching between the resonator and the amplifier and to attain the optimal operation condition of SQUID, $k^2Q_L>1$, which was confirmed by the observation of steps on the resonance curves. For the SQUID of Fig. 3 and Table I, we measured the white noise dependence on temperature, and calculated the corresponding energy densities. Here, for simplicity, we took the effective noise temperature of the tank circuit to be the same as the operation temperature of the SQUID. The results are shown in Fig. 4. The open squares are the experimental data after subtracting the background noise from the amplifier. The current noise from the integrator was not taken into account. The background noise was approximately measured by terminating the cold end of the 50 Ω cable with a 50 Ω resistor. The inset in Fig. 4 shows the measured white flux noise dependence on temperature, which includes the background noise. The minimum of white flux noise was $S_\Phi^{1/2}=12.7\mu\Phi_0/\sqrt{\text{Hz}}$. After subtracting the background noise of the electronic, the minimum energy resolution was about 8×10^{-31} J/Hz. We note that at $T<74$ K, the flux noise $S_\phi^{1/2}$ increases as the temperature decreases. This is caused, at least in part, by the decrease in temperature of the transfer function $|\partial V/\partial\Phi|$. This occurs in the temperature range where β increases and the frequency modulation decreases since the transition from dispersive to hysteretic mode of rf SQUID operation is approached. We note that $S_\phi=S_v/|\partial V/\partial\Phi|^2$ where S_v is the voltage noise.

For two other SQUID samples, Nos. 1 and 3 in Table II, we also measured the temperature dependence of flux noise. These two samples showed similar behavior as in Fig. 4. After subtracting the background noise of the electronics, the resulting energy resolution data are given in Table III.

The formulated version of rf SQUID's theory[10] is strictly valid for amplitude demodulation while we used synchronous detection by a mixer. We show in Sec. III D that at optimal operating conditions the contribution of the phase signal to the transfer function is small, so that the theory is a good approximation also when synchronous detection is used. In Fig. 4, the solid dots are values of ϵ calculated from theory using the indirectly measured rf SQUID parameters from Table I. We can see that theory and experiment show a good agreement. Good agreement is confirmed also by data of sample No. 3 in Table III, which has the same inductance of 260 pH, much higher than L_F. In the large inductance samples, the optimal energy resolution was obtained at β, much larger than 1, in the range where the frequency modulation is near maximum, i.e., the SQUID is highly dispersive. In contrast, for sample No. 1 of Table III, which had the smaller inductance of 150 pH, the optimum β was only somewhat larger than 1.

D. Role of phase signal in rf SQUID using a mixer as detector

In our described measurements, we used electronics with phase-sensitive synchronous detection by a mixer.[16] If a mixer is used as a signal detector, both the amplitude and the phase signals are detected. However, the explicit expressions of Chesca's theory were formulated for the amplitude signal only.[10] It was appropriate, therefore, to verify whether the

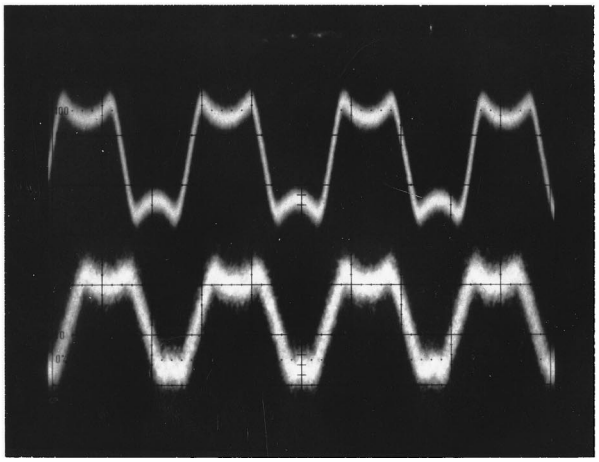

(a)

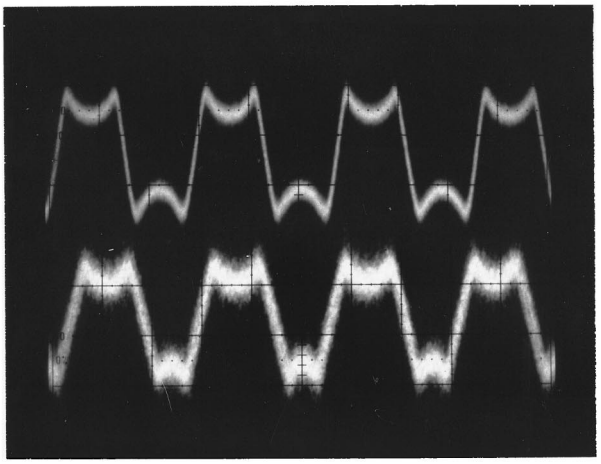

(b)

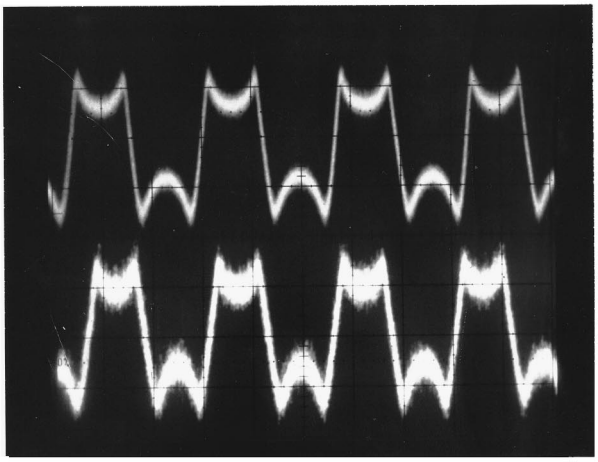

(c)

FIG. 5. Comparison of $V-\Phi$ curves obtained using mixer (upper) and diode (lower) as detector at three different temperatures. All curves have the same ordinate scale.

additional phase signal could cause a significant deviation of our experimental results from those obtained in the case of amplitude detection by a diode.

The comparative analysis of synchronous and amplitude detection was summarized by Danilov and Likharev.[20] They showed that for the nonhysteretic SQUID one should not expect any significant change of the SQUID output signal.

TABLE III. Energy resolution and optimum β for samples of Table II.

Sample No.	Optimum β	Minimum ϵ_{expt} ($\times 10^{-31}$ J/Hz)	$\epsilon_{\text{expt}}-\epsilon_{\text{th}}$ at 77 K ($\times 10^{-31}$ J/Hz)
1	~1.1	9.6	4.34
3	~2	6.5	2.33

To study the role of phase signal in rf SQUID, we measured $V-\Phi$ curves of the same SQUID using both the synchronous and the diode detector. The loop inductance of this SQUID was $L_s \cong 225$ pH and the resonance frequency of the resonator was about 610 MHz. In Fig. 5, we compare oscilloscope traces obtained with the mixer (upper trace) and diode (lower trace) at three different temperatures. All traces have the same ordinate scale. Here, the $V-\Phi$ curves were optimized for flux noise measurement. We can see that the waveforms (shape and amplitude) obtained using the two different detectors are very similar. This similarity suggests that, in optimal conditions, the phase signal contribution to the SQUID's transfer function $|\partial V/\partial \Phi|$ is small in comparison to the contribution from the amplitude signal. For that reason, the results of the analytical approach developed in Ref. 10 for the amplitude detection may well be applied also to the case when a mixer is used as detector in the SQUID readout electronics. The higher noise content in the traces obtained using the diode detector is attributed, at least in part, to the use of nonoptimized breadboard electronics constructed specifically for this measurement.

IV. CONCLUSIONS

We have shown experimentally that in the presence of large thermal fluctuations the HTS rf SQUIDs operate in nonhysteretic mode for β values up to about 3.6, which is consistent with the prediction of Chesca's theory. By measuring AFCs and using the expressions derived from theory, we could determine all rf SQUID parameters. The derived junction's I_c and R_n were in good agreement with direct measurements of the junction, thus confirming the validity of the theory. As predicted theoretically, the optimal energy sensitivity was obtained at $\beta > 1$ for a highly dispersive SQUID, in contrast to the situation at low temperatures where the optimum corresponds to $\beta \cong 1$. In optimum operation conditions, and with synchronous detection (mixer as detector), the phase signal contribution to the transfer function is small compared with the amplitude signal contribution. Hence, the use of theoretical expressions derived for the amplitude signal is justified.

ACKNOWLEDGMENTS

The authors thank R. Otto and N. Wolters for the development of the rf SQUID electronics and assistance in its use. They are also grateful to J. Schubert and W. Zander for providing the YBCO films, S. G. Wang for providing several SQUID samples, F.-J. Schröteler for help in photolithography, R. Dittmann for help in measurements of r_d, and R.

Hohmann for assistance in solving many experimental problems. They gratefully acknowledge discussions with M. Siegel and D. F. He.

[1] A. H. Siver and J. E. Zimmerman, Phys. Rev. **157**, 317 (1967).
[2] J. Kurkijärvi, J. Appl. Phys. **44**, 4191 (1973).
[3] L. D. Jackel and R. A. Buhrman, J. Low Temp. Phys. **19**, 201 (1975).
[4] T. Ryhänen, H. Seppä, R. Ilmonieni, and J. Knuutila, J. Low Temp. Phys. **76**, 287 (1989).
[5] J. Clarke, in *SQUID Sensors: Fundamentals, Fabrication and Applications* edited by H. Weinstock (Kluwer, Dordrecht, 1996), p. 43.
[6] C. M. Falco and W. H. Parker, J. Appl. Phys. **46**, 3238 (1975).
[7] E. Il'ichev, V. Zakosarenko, R. P. J. Ijsselsteijn, and V. Schultze, J. Low Temp. Phys. **106**, 503 (1997).
[8] Y. Zhang *et al.*, Appl. Phys. Lett. **71**, 704 (1997).
[9] Y. Zhang *et al.*, Appl. Supercond. **6**, 7 (1998).
[10] B. Chesca, J. Low Temp. Phys. **110**, 963 (1998).
[11] V. I. Shnyrkov, V. A. Klus, and G. M. Tsoi, J. Low Temp. Phys. **39**, 477 (1980).
[12] I. M. Dmitrenko, G. M. Tsoi, V. I. Shnyrkov, and V. V. Kartsovnik, J. Low Temp. Phys. **49**, 417 (1982).
[13] H. Fuke, K. Saitoh, T. Utagawa, and Y. Enomoto, Jpn. J. Appl. Phys., Part 2 **35**, L1582 (1996).
[14] W. Zander and J. Schubert, Forschungszentrum Jülich (unpublished).
[15] H. R. Yi, Z. G. Ivanov, D. Winkler, Y. M. Zhang, H. Olin, P. Larsson, and T. Claeson, Appl. Phys. Lett. **65**, 1177 (1994).
[16] D. Duret, P. Bernard, and D. Zentatti, Rev. Sci. Instrum. **46**, 474 (1975).
[17] In-house developed, optimized rf SQUID electronics, model V2.0.
[18] K. K. Likharev, *Dynamics of Josephson Junctions and Circuits* (Gordon and Breach, Amsterdam, 1986), p. 116.
[19] In our washer rf SQUID, step–edge junctions were formed (upon the film deposition) at sharp edges of a steep walled pit etched in the substrate. In a microbridge patterned across the pit, up to four junctions can exist in series. However, often enough, one of these has a much lower I_c than the rest, and it is that junction which then determines the SQUID behavior. With more than one junction active, such characteristics would not be obtained.
[20] V. V. Danilov and K. K. Likharev, Sov. Phys. Tech. Phys. **20**, 697 (1976); in *SQUID '80*, edited by H. D. Hahlbohm and H. Lübbig (Walter de Gruyter, Berlin, 1980), pp. 473–507.
[21] Ya. S. Greenberg, J. Low Temp. Phys. **114**, 297 (1999).